FMRP sustains presynaptic function via control of activity-dependent bulk endocytosis

Neurobiology of Disease

FMRP Sustains Presynaptic Function via Control of Activity-Dependent Bulk Endocytosis

Katherine Bonnycastle,[1,2,3] **Peter C. Kind,**[1,2,3] **and Michael A. Cousin**[1,2,3]

[1]Centre for Discovery Brain Sciences, University of Edinburgh, Edinburgh EH8 9XD, Scotland, United Kingdom, [2]Patrick Wild Centre, University of Edinburgh, Edinburgh EH8 9XD, Scotland, United Kingdom, and [3]Simons Initiative for the Developing Brain, Hugh Robson Building, University of Edinburgh, Edinburgh EH8 9XD, Scotland, United Kingdom

Synaptic vesicle (SV) recycling is essential for the maintenance of neurotransmission, with a number of neurodevelopmental disorders linked to defects in this process. Fragile X syndrome (FXS) results from a loss of fragile X mental retardation protein (FMRP) encoded by the *FMR1* gene. Hyperexcitability of neuronal circuits is a key feature of FXS, therefore we investigated whether SV recycling was affected by the absence of FMRP during increased neuronal activity. We revealed that primary neuronal cultures from male *Fmr1* knock-out (KO) rats display a specific defect in activity-dependent bulk endocytosis (ADBE). ADBE is dominant during intense neuronal activity, and this defect resulted in an inability of *Fmr1* KO neurons to sustain SV recycling during trains of high-frequency stimulation. Using a molecular replacement strategy, we also revealed that a human FMRP mutant that cannot bind BK channels failed to correct ADBE dysfunction in KO neurons, however this dysfunction was corrected by BK channel agonists. Therefore, FMRP performs a key role in sustaining neurotransmitter release via selective control of ADBE, suggesting intervention via this endocytosis mode may correct the hyperexcitability observed in FXS.

Key words: **endocytosis; FMRP; fragile X syndrome; presynapse; vesicle**

Significance Statement

Loss of fragile X mental retardation protein (FMRP) results in fragile X syndrome (FXS), however whether its loss has a direct role in neurotransmitter release remains a matter of debate. We demonstrate that neurons lacking FMRP display a specific defect in a mechanism that sustains neurotransmitter release during intense neuronal firing, called activity-dependent bulk endocytosis (ADBE). This discovery provides key insights into mechanisms of brain communication that occur because of loss of FMRP function. Importantly it also reveals ADBE as a potential therapeutic target to correct the circuit hyperexcitability observed in FXS.

Introduction

Information communication between neurons requires the synchronous fusion of neurotransmitter-containing synaptic vesicles (SVs) during neuronal activity. SVs that are mobilized by action potentials (APs) are termed the recycling pool, which can be subdivided into the readily releasable pool (RRP; comprising primed fusion-ready SVs) and the reserve pool (SVs only mobilized during high neuronal activity; Alabi and Tsien, 2012). Several SV endocytosis modes are sequentially recruited by increasing stimulus intensity to replenish these SV pools (Chanaday et al., 2019). Ultrafast endocytosis is dominant during sparse neuronal activity (Watanabe et al., 2013), whereas clathrin-mediated endocytosis becomes prevalent during AP trains (Granseth et al., 2006). Both ultrafast and clathrin-mediated endocytosis saturate during heightened neuronal activity (López-Murcia et al., 2014; Soykan et al., 2017), and under these conditions, activity-dependent bulk endocytosis (ADBE) is the dominant endocytosis mode (Clayton et al., 2008). ADBE generates large endosomes directly from the plasma membrane, from which SVs are formed to replenish the reserve pool (Richards et al., 2000; Cheung et al., 2010).

The translation repressor fragile X mental retardation protein (FMRP) is located in several cellular compartments including central nerve terminals, where it controls the expression of a cohort of presynaptic proteins (Darnell and Klann, 2013). It also has protein synthesis-independent presynaptic functions, such as mediating ion channel gating, activation and density (reviewed

Received Apr. 19, 2021; revised Dec. 22, 2021; accepted Dec. 23, 2021.

Author contributions: P.C.K. and M.A.C. designed research; K.B. performed research; K.B. analyzed data; K.B. wrote the first draft of the paper; K.B., P.C.K., and M.A.C. edited the paper; K.B., P.C.K., and M.A.C. wrote the paper.

This work was supported by grants from the Simons Foundation (529508), The RS McDonald fund, and a College of Medicine and Veterinary Medicine studentship. We thank Jennifer Darnell for expert advice and Steven Mitchell for excellent technical assistance.

The authors declare no competing financial interests.

Correspondence should be addressed to Michael A. Cousin at m.cousin@ed.ac.uk.

https://doi.org/10.1523/JNEUROSCI.0852-21.2021

in Ferron, 2016). For example, FMRP interacts with Slack potassium channels (Brown et al., 2010), N-type calcium channels (Ferron et al., 2014) and large conductance voltage and calcium-gated big potassium (BK) channels (Deng et al., 2013; Deng and Klyachko, 2016; Kshatri et al., 2020). The absence of FMRP at CA3-CA1 hippocampal synapses leads to reduced BK channel activity and excessive AP broadening (Deng et al., 2013; Wang et al., 2014; Deng and Klyachko, 2016), resulting in increased presynaptic calcium influx during high-frequency stimulation (Deng et al., 2011, 2013). These synapses also display altered short-term plasticity, but only during periods of heightened activity (Deng et al., 2011; Klemmer et al., 2011). Therefore, presynaptic phenotypes that occur in the absence of FMRP are only revealed during intense neuronal activity (Deng et al., 2011, 2013; Ferron et al., 2014).

Hyperexcitability of neuronal circuits is a key feature of fragile X syndrome (FXS; Booker et al., 2019; Das Sharma et al., 2020), one of the most common monogenic causes of intellectual disability (ID) and autism spectrum disorder (Mefford et al., 2012). Most FXS cases are caused by a CGG trinucleotide expansion in the 5′ untranslated region of the *FMR1* gene which encodes FMRP, leading to hypermethylation of the promoter and silencing of the *FMR1* gene. Additionally, a point mutation which disrupts polyribosome binding (I304N), is sufficient to cause FXS (Feng et al., 1997), whereas a different mutation in FMRP that is unable to bind to and regulate BK channels (R138Q) has been identified in different individuals that display ID and FXS phenotypes (Collins et al., 2010; Myrick et al., 2015; Diaz et al., 2018; Sitzmann et al., 2018).

Since FMRP appears to be required for optimal presynaptic function specifically during intense neuronal activity, we determined whether SV recycling was disproportionately impacted under these conditions in primary neuronal cultures derived from an *Fmr1* knock-out (KO) rat model (Asiminas et al., 2019). No significant defect in either SV exocytosis or endocytosis was observed, however *Fmr1* KO neurons displayed a robust defect in ADBE. This dysfunction reduced presynaptic performance during periods of intense neuronal activity. Finally, molecular replacement studies with human FMRP mutants revealed that the ADBE defect was because of loss of BK channel interactions and that BK channel activators could restore normal function in *Fmr1* KO neurons.

Materials and Methods

Materials

Unless otherwise specified, all cell culture reagents were obtained from Invitrogen. Fetal bovine serum was from BioSera. Papain was obtained from Worthington Biochemical. All other reagents were obtained from Sigma-Aldrich unless specified. Rabbit anti-SV2A was obtained from Abcam (ab32942 RRID: AB_778192). Guinea-pig anti-vGLUT (135304 RID:AB_887878) and rabbit anti-vGAT (274102 RRID:AB_2620000) were obtained from SYSY. Anti-rabbit Alexa Fluor 488 (A11008 RRID: AB_143165), anti-guinea pig Alexa Fluor 568 (A11075 RRID:AB_2534119), and donkey anti-rabbit Alexa Fluor 647 (A32795 RRID:AB_2866496) were obtained from Invitrogen. The mCerN1 (empty vector) was constructed as previously described (Cheung et al., 2010). Synaptophysin-pHluorin (sypHy) was provided by Prof. L. Lagnado (University of Sussex, UK). pGP-CMV-GCamP6f was a gift from Douglas Kim and the GENIE project (Addgene plasmid #40755; RRID: Addgene_40755; Chen et al., 2013). Synaptophysin-mOrange2 was from Prof. Shigeo Takamori (Doshisha University, Koyto, Japan). hEGFP-FMRP isoform 1, was obtained from Dr. B. Bardoni (Institut National de la Santé et de la Recherche Médicale, Institute Pharmacology Moléculaire Et Cellulaire Centre National de la Recherche Scientifique; Khayachi et al., 2018). hEGFP-$FMRP_{R138Q}$ and hEGFP-$FMRP_{I304N}$ were generated using site-targeted mutagenesis (R138Q forward primer GTGCCAGAAGACTTACAGCAAATGTGTGCCAAA; reverse primer TTTGGCACACATTTGCTGTAAGTCTTCTGGCAC: I304N forward primer AAAAATGGAAAGCTGAATCAGGAGATTGTGGAC; reverse GTCCACAATCTCCTGATTCAGCTTTCCATTTTT (mutated bases underlined). The base change was confirmed by Source Bioscience Sanger Sequencing.

Primary neuronal culture

Animal work was performed in accordance with the UK Animal (Scientific Procedures) Act 1986, under Project and Personal License authority and was approved by the Animal Welfare and Ethical Review Body at the University of Edinburgh (Home Office project license 7008878). Specifically, all animals were killed by schedule 1 procedures in accordance with United Kingdom Home Office Guidelines; adults were killed by exposure to CO_2 followed by decapitation, whereas embryos were killed by decapitation followed by destruction of the brain.

Heterozygous LE-*Fmr1*$^{em1/PWC}$ female rats (Asiminas et al., 2019) were mated with wild-type (WT) males to produce either *Fmr1* KO or WT males. Male embryos were taken at e18.5–e19.5 for hippocampal dissection. Hippocampi from each embryo were processed separately to avoid contamination across genotypes. Dissociated primary hippocampal cultures were prepared from embryos as previously described (Zhang et al., 2015). Briefly, isolated hippocampi were digested in a 10 U/ml papain solution (Worthington Biochemical, LK003178) at 37°C for 20 min. The papain was then neutralized using DMEM F12 (ThermoFisher Scientific, 21331-020) supplemented with 10% fetal bovine serum (BioSera, S1810-500) and 1% penicillin/streptomycin (ThermoFisher Scientific, 15140-122). Cells were triturated to form a single cell suspension and plated at 5×10^4 cells (with the exception of single cell tetramethylrhodamine (TMR)-dextran uptake experiments, 2.5×10^4 cells) per coverslip on laminin (10 µg/ml; Sigma-Aldrich, L2020) and poly-D-lysine (Sigma-Aldrich, P7886)-coated 25-mm glass coverslips (VWR International Ltd). Cultures were maintained in Neurobasal media (ThermoFisher Scientific, 21103-049) supplemented with 2% B-27 (ThermoFisher Scientific, 17504-044), 0.5 mM L-glutamine (ThermoFisher Scientific, 25030-024), and 1% penicillin/streptomycin. After 2–3 d *in vitro* (DIV), 1 μM cytosine arabinofuranoside (Sigma-Aldrich, C1768) was added to each well to inhibit glial proliferation. Hippocampal neurons were transfected with sypHy or co-transfected with both GCamP6f and synaptophysin-mOrange2 at DIV7 using Lipofectamine 2000 (ThermoFisher Scientific, 11668027) as per manufacturer's instructions and imaged at DIV13–DIV15. For single-cell TMR-dextran experiments, neurons were transfected with mCerN1 or hEGFP-FMRP constructs using Lipofectamine 2000 3 d before imaging at DIV13–DIV15.

SypHy and GCaMP6f imaging

SypHy-transfected neurons were visualized at 500-nm band pass excitation with a 515-nm dichroic filter and a long-pass >520-nm emission filter on a Zeiss Axio Observer D1 inverted epifluorescence microscope. Images were captured using an AxioCam 506 mono camera (Zeiss) with a Zeiss EC Plan Neofluar 40×/1.30 oil immersion objective. Image acquisition was performed using Zen Pro software (Zeiss). Hippocampal cultures were mounted in a Warner Instruments imaging chamber with embedded parallel platinum wires (RC-21BRFS) and challenged with field stimulation using a Digitimer LTD MultiStim system-D330 stimulator (current output 100 mA, current width 1 ms) either at 10 Hz for 30 s, 40 Hz for 10 s, or 4 × 40 Hz for 10 s with 5-min intervals between trains. Imaging time courses were acquired at 4-s intervals while undergoing constant perfusion with imaging buffer [119 mM NaCl, 2.5 mM KCl, 2 mM $CaCl_2$, 2 mM $MgCl_2$, 25 mM HEPES, and 30 mM glucose at pH 7.4, supplemented with 10 μM 6-cyano-7-nitroquinoxaline-2,3-dione (Abcam, ab120271) and 50 μM DL-2-amino-5-phosphonopentanoic acid (Abcam, ab120044)]. Alkaline buffer (50 mM NH_4Cl substituted for 50 mM NaCl) was used to reveal the maximal pHluorin response.

The size of the different functional SV pools in hippocampal neurons was measured by stimulating sypHy-transfected neurons for increasing durations in the presence of 1 μM bafilomycin A1 (Cayman Chemical Company, 11038). The RRP was mobilized by 40 APs (20 Hz), and 10 s later, the remainder of the recycling pool mobilized with a second challenge of 1600 APs (20 Hz). The resting pool was revealed by application of NH_4Cl buffer.

Hippocampal neurons co-transfected with GCamP6f and synaptophysin-mOrange2 were mounted on a Zeiss Axio Observer D1 microscope as described above and were visualized at 500-nm band pass excitation with a 515 nm dichroic filter and a long-pass >520 nm. An image of transfected neurons was acquired before 40 Hz (10 s) stimulation using 556/25 nm excitation and 630/98 nm emission bandpass filters (Zeiss) to view synaptophysin-mOrange2 marking of nerve terminals. Imaging time courses were acquired at 2-s intervals while undergoing constant perfusion with imaging buffer.

Time traces were analyzed using the FIJI distribution of ImageJ (National Institutes of Health; NIH). Images were aligned using the Rigid body model of the StackReg plugin (https://imagej.net/StackReg). Nerve terminal fluorescence was measured using the Time Series Analyser plugin (https://imagej.nih.gov/ij/plugins/time-series.html). Regions of interest (ROIs) five pixels in diameter were placed over nerve terminals that responded to the electrical stimulus. The proportion of ROIs that were responsive to stimulation was not different between genotypes (for sypHy experiments: WT 28.6 ± 5.4; KO 26.1 ± 6.2% responsive synapses; for GCamP6f experiments: WT 92.0 ± 5.2%; KO 85.9 ± 7.3% of synaptophysin-mOrange2 puncta respond to the field potential stimulus). A response trace was calculated for each cell by averaging the individual traces from each selected ROI $\Delta F/F_0$. Baseline fluorescence was subtracted from GCamP6f time traces to correct for high background fluorescence. For sypHy time traces, fluorescence decay time constants (tau, τ, s) were calculated by fitting a monoexponential decay curve to data from the time point after the end of electrical stimulation.

TMR-dextran uptake

TMR-dextran (ThermoFisher Scientific, D1842) uptake was performed as described previously (Nicholson-Fish et al., 2015). Neurons were mounted on a Zeiss Axio Observer D1 microscope as described above before challenging with 400 APs (40 Hz) in the presence of 50 μM of TMR-dextran (40,000 MW) in imaging buffer. Where the experiment was performed with BK channel modulators, neurons were incubated in 50 μM of TMR-dextran and either DMSO (Sigma-Aldrich, D8418), 10 μM NS 11021 (Bio-Techne Ltd, 4788/10), or 10 μM Paxilline (Bio-Techne Ltd, 2006/10) for 120 s before stimulation. The TMR-dextran solution was immediately washed away after stimulation terminated, and images were acquired using 556/25-nm excitation and 630/98-nm emission bandpass filters (Zeiss) while undergoing constant perfusion. Per coverslip of cells, three to six different fields of view were imaged. The TMR-dextran puncta in each image were quantified using the Analyze Particles plugin of ImageJ (NIH; https://imagej.nih.gov/ij/developer/api/ij/ij/plugin/filter/ParticleAnalyzer.html) to select and count particles of 0.23–0.91 μm^2.

Where TMR-dextran uptake was performed on transfected cultures, WT and KO neurons were transfected 3 d before imaging with mCer-N1 plus either hEGFP-$FMRP_{WT}$, hEGFP-$FMRP_{I304N}$ or hEGFP-$FMRP_{R138Q}$ or mCer-N1 alone. Transfected axons were visualized on DIV13–DIV15 at both 430- and 500-nm excitation (long-pass emission filter >520 nm) to ensure co-transfection. Images of transfected neurons and of TMR-dextran were acquired using 470/27- and 556/25-nm double band pass filters and emission filters 512/30 and 630/98 nm, respectively (Zeiss). Per coverslip of cells, two to eight neurons were imaged. Axon length was calculated using the Simple Neurite Tracer plugin of ImageJ (NIH; https://imagej.net/SNT). TMR-dextran puncta (0.23–0.91 μm^2) were counted along transfected axons with the final value normalized for axon length. For all experiments, for each condition, at least one unstimulated coverslip was imaged to correct for the background level of TMR-dextran uptake.

Immunofluorescence staining

Immunofluorescence staining was performed as previously described (Nicholson-Fish et al., 2015). Briefly, hippocampal neurons were fixed with 4% paraformaldehyde (Sigma-Aldrich, 47608) in PBS for 15 min. Excess paraformaldehyde was quenched with 50 mM NH_4Cl in PBS. Cells were then permeabilized in 1% bovine serum albumin (BSA; Roche Diagnostics GmbH, 10735078001) in PBS-Triton X-100 0.1% solution for 5 min and blocked in 1% BSA in PBS at room temperature for 1 h. After blocking, cells were incubated in rabbit anti-SV2A (1:200 dilution) for 1 h, after which the cultures were washed with PBS and incubated with fluorescently conjugated secondary antibodies (anti-rabbit Alexa Fluor 488; 1:1000 dilution) for 1 h. The coverslips were mounted on slides for imaging with FluorSave (Millipore, 345789). SV2A puncta were visualized at 500-nm band pass excitation with a 515-nm dichroic filter and a long-pass >520-nm emission filter on a Zeiss Axio Observer D1 inverted epifluorescence microscope. Images were captured using an AxioCam 506 mono camera (Zeiss) with a Zeiss EC Plan Neofluar 40×/1.30 oil immersion objective. SV2A puncta in each image were quantified using the Analyze Particles plugin of ImageJ to select and count particles of 0.23–3.18 μm^2.

Fluorescein (FITC)-dextran uptake

Hippocampal neurons were exposed to FITC-dextran (40,000 MW, 50 μM) in imaging buffer during challenge with 400 APs (40 Hz) in an identical manner to TMR-dextran uptake. Neurons underwent an identical immunofluorescence staining protocol to that described above, with the exception that neurons were incubated with guinea pig anti-vGLUT and rabbit anti-vGAT primary antibodies (both at 1:1000 dilution) and goat anti-guinea pig Alexa Fluor 568 and donkey anti-rabbit Alexa Fluor 647 (1:1000 dilution). Fluorescent neurons were visualized using an AxioObserver Z1 inverted epifluorescence microscope and an AxioCam 506 mono camera. Excitation was provided by a Colibri 7 Solid-State Light Source using 475-, 555-, and 630-nm wavelengths, respectively. Emission was monitored using the following bandpass filters 525/50, 605/70, and 690/50 nm.

Per coverslip of cells, three to nine different fields of view were imaged and FIJI was used for image processing. The background was subtracted from all images using the Rolling Ball algorithm (https://imagej.net/plugins/rolling-ball-background-subtraction). Images with vGLUT and vGAT staining were auto-thresholded using Otsu's algorithm (Otsu, 1979). Masks were then generated of particles sized 5–150 px, representing antibody staining at nerve terminals. For FITC images, the threshold was set at 5, 255 and masks with particles 3–19 px were generated, representing internalized FITC-dextran. To determine the overlap between masks, a combined image was created using image calculator (NIH) and overlapping particles were counted.

Horseradish peroxidase (HRP) uptake

Hippocampal cultures were mounted in the RC-21BRFS stimulation chamber and challenged with 400 APs (40 Hz) in the presence of 10 mg/ml HRP (Sigma-Aldrich, P8250) supplemented imaging buffer. Immediately following the end of stimulation, cultures were washed in imaging buffer to remove noninternalized HRP and fixed with a solution of 2% glutaraldehyde (Electron Microscopy Sciences, 16019) in PBS. After washing in 0.1 M Tris buffer, HRP was developed with 0.1% 3,3'-diaminobenzidine (Fluka Chemica, 22204001) and 0.2% v/v hydrogen peroxide (Honeywell, 216763) in Tris buffer. After further washing in Tris buffer, cultures were then stained with 1% osmium tetroxide (TAAB laboratory and microscopy, O015/1) for 30 min. Samples were then dehydrated using an ethanol series and polypropylene oxide (Electron Microscopy Sciences, 20411) and embedded using Durcupan resin (Sigma-Aldrich, 44610). Samples were sectioned, mounted on grids, and viewed using an FEI Tecnai 12 transmission electron microscope. Intracellular structures that were <61 nm in diameter were arbitrarily designated to be SVs, whereas larger structures were considered endosomes. The area of individual endosomes was obtained by tracing the circumference using the freehand selections tool in ImageJ and measuring the resulting area. Typically, 30 fields of view were acquired for one coverslip of cells. In nerve terminals that contained HRP, the average number of HRP-labeled endosomes and SVs per nerve terminal was calculated for each coverslip and represents the experimental n.

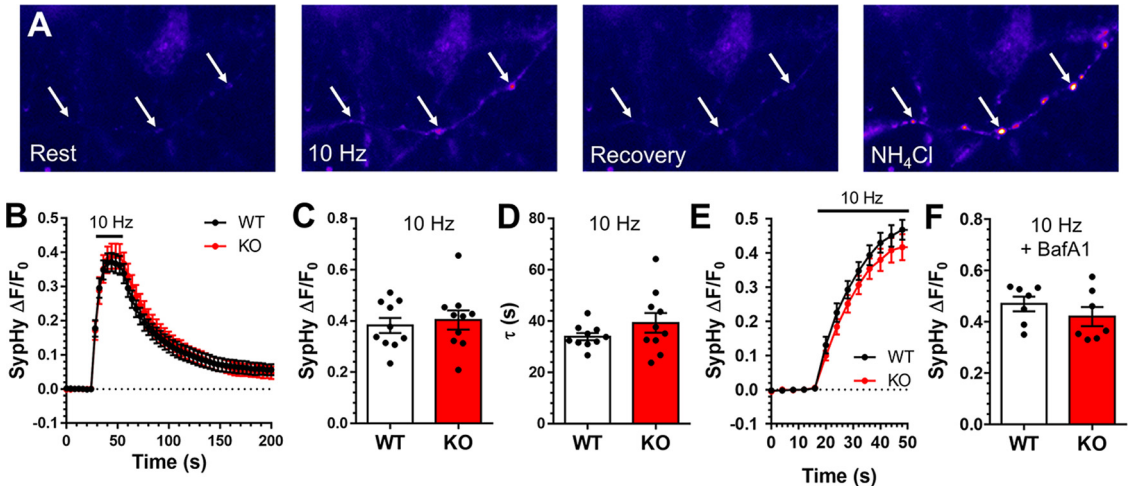

Figure 1. *Fmr1* KO hippocampal neurons show no obvious defect in SV recycling during low-frequency stimulation. ***A–D,*** Hippocampal neurons derived from either *Fmr1* KO or WT littermate controls were transfected with sypHy on DIV7 and imaged DIV13–DIV15. Transfected neurons were challenged with a train of 300 APs (10 Hz) and left to recover for 3 min before exposure to an alkaline buffer (NH_4Cl). ***A***, Representative images of nerve terminals (indicated by arrows) transfected with sypHy at different points during this experiment (Rest, 10 Hz, Recovery, and NH_4Cl). Scale bar: 5 μm. ***B***, Mean trace displaying the average sypHy fluorescent response of WT (black) and KO (red) hippocampal neurons in response to stimulation ± SEM. Traces are $\Delta F/F_0$ and are presented as a fraction of the total SV pool, revealed by NH_4Cl application. Bar indicates the period of stimulation. ***C***, Mean sypHy peak height ± SEM during stimulation. ***D***, Mean sypHy retrieval time constants (τ ± SEM) following stimulation. $n = 10$ for both WT and KO, unpaired Student's *t* test, ***C***, $p = 0.65$; ***D***, $p = 0.21$. ***E***, ***F***, Hippocampal neurons were transfected, imaged, and stimulated in an identical manner to above except neurons where exposed to 1 μ_M bafilomycin A1. ***E***, Mean trace displays the average sypHy response to 300 APs delivered at 10 Hz ($\Delta F/F_0$ as a fraction of the total SV pool, revealed by NH_4Cl). Bar indicates stimulation period. ***F***, Mean sypHy peak height during 10-Hz stimulation ± SEM, $n = 7$ for both WT and KO, unpaired Student's *t* test, $p = 0.31$.

Experimental design and statistical analysis

Microsoft Excel (Microsoft) and Prism 6 software (GraphPad Software Inc.) were used for data processing and analysis. The experimenter was blinded to genotype during the acquisition and to both the genotype and drug treatment or transfection condition during data analysis. For all figures, results are presented with error bars as ±SEM, and the n for each condition represents the number of coverslips imaged. For all assays, cells were obtained from at least two cultures, each containing at least three independent preparations from individual embryos. In sypHy assays, at least 10 ROIs were collected from each coverslip. The number of ROIs examined was comparable for all experiments. Normality was determined using a D'Agostino and Pearson omnibus normality test. For comparison between genotypes, an unpaired Student's *t* test was performed where data followed a normal distribution, with a Mann–Whitney test performed for those that did not. For comparison between more than two conditions, a one-way ANOVA was performed, whereas a two-way ANOVA was performed for comparison between genotypes across multiple stimulation trains. For both one-way and two-way ANOVA tests, results were corrected for multiple comparisons.

Results

Fmr1 KO hippocampal neurons show no obvious defect in SV recycling

FMRP is proposed to control SV fusion (Ferron et al., 2014), presynaptic AP duration (Deng et al., 2011), and short-term synaptic plasticity (Deng et al., 2011; Klemmer et al., 2011) in different murine models. To determine whether SV exocytosis or endocytosis were altered in a recently generated *Fmr1* KO rat model (Asiminas et al., 2019), we examined SV recycling using sypHy in primary hippocampal cultures from KO or WT littermate controls. SypHy consists of the SV protein synaptophysin with a pH-sensitive EGFP (pHluorin) fused to an intraluminal loop (Granseth et al., 2006). Since sypHy reports the pH of its immediate environment, an exocytosis-dependent increase in its fluorescence signal is observed during SV fusion (Fig. 1*A*,*B*). After endocytosis, sypHy fluorescence is quenched by SV acidification. This loss of fluorescence is an estimate of the kinetics of SV endocytosis, since this is rate-limiting (Atluri and Ryan, 2006; Granseth et al., 2006). When WT neurons were challenged with a train of 300 APs delivered at 10 Hz, they displayed a characteristic sypHy response, with an evoked increase in fluorescence followed by an exponential poststimulation decrease to baseline (Fig. 1*B*). To determine the amount of exocytosis as a proportion of the total SV pool, fluorescence traces were normalized to the sypHy response in the presence of an alkaline solution (to reveal the maximal unquenched signal; Fig. 1*B*). No significant difference in this parameter was observed when WT and KO were compared (Fig. 1*C*). The lack of effect was confirmed using the vacuolar-type ATPase inhibitor bafilomycin A1 which allows SV exocytosis to be reported without confounding input from SV endocytosis (Sankaranarayanan and Ryan, 2001; Fig. 1*E*,*F*). The time constant, τ, of SV endocytosis was also not significantly different between WT and KO neurons (Fig. 1*D*). Therefore, loss of FMRP does not impair SV exocytosis or endocytosis during low-frequency stimulation.

Previous studies examining loss of FMRP function revealed presynaptic defects during high-frequency stimulation (Deng et al., 2011; Ferron et al., 2014; Wang et al., 2014). Therefore, we next examined sypHy responses evoked by a train of 400 APs delivered at 40 Hz (Fig. 2). Under these stimulation conditions, there was no difference in either the extent of SV exocytosis, measured with or without bafilomycin A1 (Fig. 2*B*,*D*,*E*) or the kinetics of SV endocytosis (Fig. 2*C*). Taken together, this indicates that deletion of *Fmr1* does not play a significant role in SV recycling during either low or high-frequency activity.

Previous studies that examined presynaptic morphology in *Fmr1* KO cultures have produced contradictory observations on the number and density of SV in nerve terminals (Deng et al., 2011; Klemmer et al., 2011). To determine whether there was any alteration in the size of functional SV pools rather than SV numbers themselves, we inhibited SV acidification with bafilomycin A1 in sypHy-transfected neurons (Sankaranarayanan and Ryan, 2001; Fig. 3). In these experiments, the RRP was mobilized

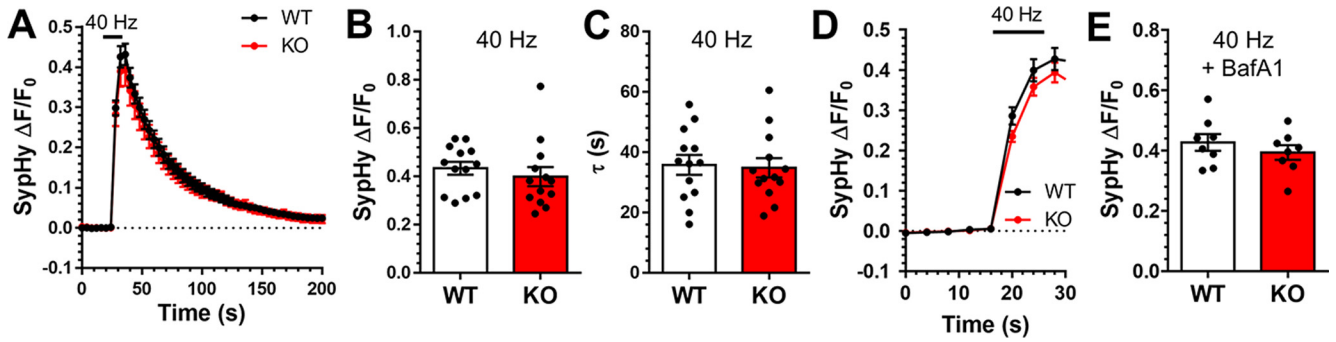

Figure 2. *Fmr1* KO hippocampal neurons show no obvious defect in SV recycling during high-frequency stimulation. ***A–C***, Hippocampal neurons derived from either *Fmr1* KO or WT littermate controls were transfected with sypHy on DIV7 and imaged DIV13–DIV15. Transfected neurons were challenged with a train of 400 APs (40 Hz) and left to recover for 3 min before exposure to an alkaline buffer (NH_4Cl). ***A***, Mean trace displaying the average sypHy fluorescent response of WT (black) and KO (red) hippocampal neurons in response to stimulation ± SEM. Traces are $\Delta F/F_0$ and are presented as a fraction of the total SV pool, revealed by NH_4Cl application. Bar indicates the period of stimulation. ***B***, Mean sypHy peak height ± SEM during stimulation. ***C***, Mean sypHy retrieval time constants (τ ± SEM) following stimulation. $n = 13$ for both WT and KO, Mann–Whitney test ***B***, $p = 0.26$; unpaired Student's *t* test ***C***, $p = 0.84$. ***D***, ***E***, Hippocampal neurons were transfected, imaged, and stimulated in an identical manner to above except neurons where exposed to 1 μM bafilomycin A1. ***D***, Mean trace displays the average sypHy response to 400 APs delivered at 40 Hz ($\Delta F/F_0$ as a fraction of the total SV pool, revealed by NH_4Cl). Bar indicates stimulation period. ***E***, Mean sypHy peak height during 40-Hz stimulation ± SEM ($n = 8$ for both WT and KO, unpaired Student's *t* test, $p = 0.38$).

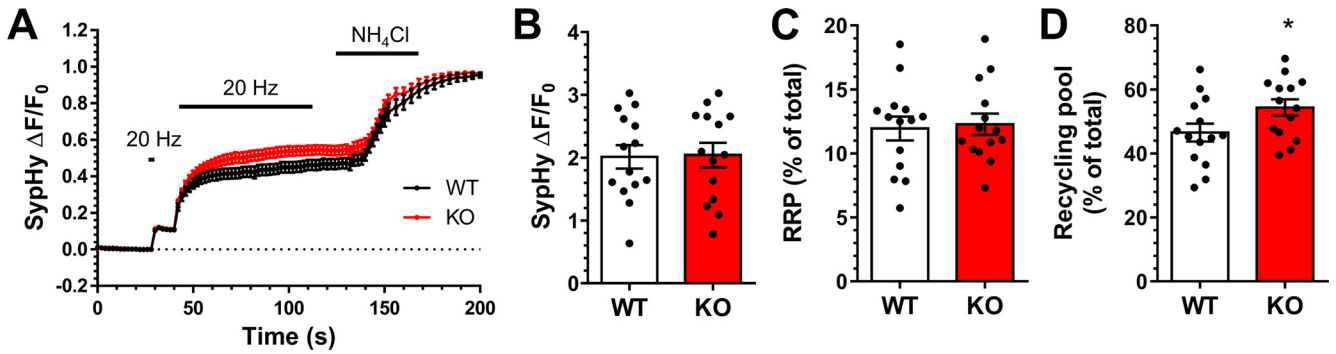

Figure 3. *Fmr1* KO hippocampal neurons have a larger recycling pool. Hippocampal neurons derived from either *Fmr1* KO or WT littermate controls were transfected with sypHy on DIV7 and imaged DIV13–DIV15 in the presence of 1 μM bafilomycin A1. Transfected neurons were challenged with two trains of APs (20 Hz, 2 s and 20 Hz 80 s) before exposure to alkaline buffer (NH_4Cl). ***A***, Mean traces displaying the average sypHy fluorescent response of WT (black) and KO (red) hippocampal neurons is displayed ± SEM. Traces are $\Delta F/F_0$ and normalized to the total SV pool, revealed by NH_4Cl application. Bars indicate periods of stimulation. ***B***, Mean sypHy fluorescence during exposure to NH_4Cl ± SEM. ***C***, Mean sypHy peak height ± SEM during 20-Hz 2-s stimulation (RRP, % of total pool). ***D***, Mean sypHy peak height ± SEM during 20-Hz 80-s stimulation (Recycling pool, % of total pool). $n = 14$ for WT and KO, unpaired Student's *t* test; ***B***, $p = 0.91$; ***C***, $p = 0.79$; ***D***, $^*p = 0.0498$.

by 40 APs (20 Hz), and the remainder of the recycling pool by 1600 APs (20 Hz). The resting pool (which cannot be mobilized by APs) was revealed by application of an alkaline solution (Fig. 3*A*). In these experiments, we observed no difference in either the size of the total SV pool (Fig. 3*B*) or the RRP between genotypes (Fig. 3*C*). However, a small, but significant, increase in the SV recycling pool was observed in *Fmr1* KO cultures (Fig. 3*D*).

Fmr1 KO hippocampal neurons display defective ADBE

Our experiments thus far have revealed that the absence of FMRP has little effect on either SV recycling or functional SV pool size. However, since presynaptic deficiencies in the absence of FMRP are only revealed during high-frequency stimulation (Deng et al., 2011; Ferron et al., 2014; Wang et al., 2014), we next assessed whether ADBE was affected in *Fmr1* KO neurons. ADBE is the dominant mode of SV endocytosis during physiological patterns of activity in dissociated neuronal culture (Clayton et al., 2008) and intact neuronal circuits (Imig et al., 2020), and in response to environmental stimuli *in vivo* (Körber et al., 2012). Therefore altered ADBE may contribute to the activity-specific changes in neurotransmission previously observed in *Fmr1* KO synapses.

ADBE was monitored optically using uptake of 40-kDa TMR-dextran, which is a fluid phase marker that is selectively accumulated via this endocytosis mode (Clayton et al., 2008). WT and *Fmr1* KO neurons were challenged with a train of 400 APs (40 Hz) to maximally trigger ADBE in the presence of TMR-dextran (Clayton et al., 2008; Nicholson-Fish et al., 2015). The number of nerve terminals that performed ADBE were revealed as discrete TMR-dextran fluorescent puncta (Fig. 4*A*,*B*). There was a significant decrease in TMR-dextran puncta in *Fmr1* KO neurons relative to WT littermate controls (Fig. 4*C*). Importantly, this phenotype was not because of synapse loss in the *Fmr1* KO cultures, since there was no difference in nerve terminal numbers as measured by staining for the SV protein SV2A (Fig. 4*D*). The absence of synapse loss was confirmed by quantifying the number of excitatory and inhibitory nerve terminals in WT and *Fmr1* KO cultures using antibodies against the glutamate and GABA transporters vGLUT and vGAT, respectively. When this analysis was performed, no significant difference in nerve terminal number was observed (Fig. 4*E*,*F*). Co-labeling with a fixable form of 40-kDa dextran (FITC-dextran) during a 400 AP train (40 Hz) confirmed the inhibition of ADBE (Fig. 4*G*), while the number of vGLUT and vGAT puncta positive for FITC-dextran was consistent with previous reports

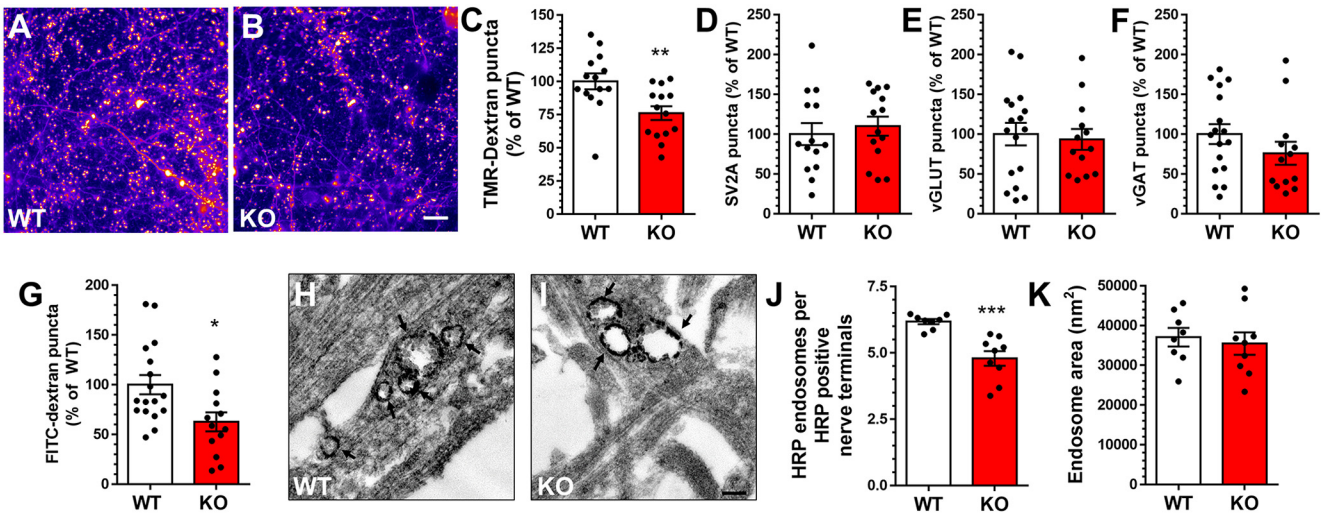

Figure 4. *Fmr1* KO hippocampal neurons show a defect in ADBE. ***A–C***, Hippocampal neurons derived from either *Fmr1* KO or WT littermate controls were challenged with a 40-Hz 10-s AP train in the presence of 50 μM TMR-dextran at DIV13–DIV15. ***A***, ***B***, Representative images of TMR-dextran-loaded nerve terminals of WT (***A***) and KO (***B***) hippocampal neurons. Scale bar: 30 µm. ***C***, Mean TMR-dextran uptake is presented as a proportion of total WT uptake ± SEM, $n = 14$ for both WT and KO, unpaired Student's *t* test $^{**}p = 0.0054$. ***D***, *Fmr1* KO neurons or WT littermate controls were fixed and stained with anti-SV2A as a marker of nerve terminals. Bar graph represents the mean number of SV2A-stained puncta for both KO and WT normalized to WT ± SEM, $n = 14$ for both WT and KO, unpaired Student's *t* test $p = 0.54$. ***E–G***, Hippocampal neurons derived from either *Fmr1* KO or WT littermate controls were challenged with a 40-Hz 10-s AP train in the presence of 50 μM FITC-dextran at DIV13–DIV15, fixed and then stained for either vGLUT or vGAT. Bar graph represents the mean number of vGLUT (***E***) or vGAT (***F***) puncta for both KO and WT (normalized to WT ± SEM, $n = 17$ for WT, $n = 13$ for KO, unpaired Student's *t* test vGLUT $p = 0.739$; vGAT $p = 0.212$). ***G***, Mean FITC-dextran uptake as a proportion of total WT uptake ± SEM, $n = 17$ for WT, $n = 13$ for KO, unpaired Student's *t* test $^{*}p = 0.012$. ***H–K***, Hippocampal neurons derived from either *Fmr1* KO or WT littermate controls were challenged with a 40-Hz 10-s AP train in the presence of 10 mg/ml HRP at DIV13–DIV15. ***H***, ***I***, Representative images of HRP-labeled endosomes and SVs in WT (***H***) and KO (***I***) nerve terminals. Black arrows in indicate HRP endosomes. Scale bar: 200 nm. ***J***, Mean HRP-labeled endosome number per nerve terminal in WT and KO cultures ± SEM in nerve terminals that contain HRP-labeled endosomes. ***K***, Mean HRP-labeled endosome areas in WT and KO ± SEM. WT $n = 8$; KO $n = 9$, unpaired Student's *t* test ***G***, $^{***}p = 0.0004$; ***H***, $p = 0.67$.

(Wenzel et al., 2012; vGLUT puncta with FITC-dextran, 4.62 ± 0.45%: vGAT puncta, 5.43 ± 0.46%, $n = 17$ WT, $n = 13$ KO). Taken together, these results reveal a small but robust decrease in the number of nerve terminals undergoing ADBE, suggesting that FMRP may be required for the optimal functioning of this mode of endocytosis.

TMR-dextran uptake reports the number of nerve terminals undergoing ADBE, not the extent to which ADBE occurs in each nerve terminal (Clayton et al., 2008). Therefore, we applied the fluid phase marker HRP during AP stimulation (40 Hz 10 s) to confirm the ADBE defect in *Fmr1* KO neurons (Fig. 4*H*,*I*). We observed a significant reduction in the number of HRP-labeled endosomes in *Fmr1* KO neurons compared with WT in nerve terminals that contained HRP (Fig. 4*J*), whereas the endosome area across both genotypes was not significantly different (Fig. 4*K*). This reduction in the generation of bulk endosomes reveals that *Fmr1* KO neurons display a specific defect in both the extent and prevalence of ADBE during intense neuronal activity.

ADBE is reduced at stimulus frequencies above 40 Hz (Clayton et al., 2008). This reduction may result from excess activity-dependent calcium influx, since this inhibits various forms of SV endocytosis in both large atypical and small central nerve terminals (von Gersdorff and Matthews, 1994; Cousin and Robinson, 2000; Wu and Wu, 2014; Leitz and Kavalali, 2016). Furthermore, it has been reported that *Fmr1* KO neurons display enhanced calcium influx during AP stimulation because of either dysfunctional BK channel function or altered trafficking of voltage-gated calcium channels (Deng et al., 2013; Ferron et al., 2014, 2020). Therefore, to determine whether activity-dependent calcium influx may underlie the depression of ADBE in *Fmr1* KO neurons, we monitored changes in presynaptic intracellular free calcium during trains of high-frequency AP stimulation. Primary cultures of both WT and *Fmr1* KO neurons were co-transfected with both the genetically-encoded reporter GCaMP6f and synaptophysin-mOrange2 (to mark nerve terminals) and were then challenged with a train of 400 APs (40 Hz). The extent of the evoked GCaMP6f response at synaptophysin-mOrange2 puncta was not significantly different when WT and *Fmr1* KO neurons were compared (Fig. 5). Therefore, the depression of ADBE observed in *Fmr1* KO neurons was not a result of increased presynaptic calcium influx during intense neuronal activity.

Defective ADBE in *Fmr1* KO neurons results in decreased presynaptic performance

Since ADBE is the dominant endocytosis mode during intense neuronal activity (Clayton et al., 2008), the impact of defective ADBE on SV exocytosis may only be revealed during patterns of high-frequency stimulation. To determine this, we monitored the amount of sypHy that visited the plasma membrane as a surrogate of neurotransmitter release in response to multiple trains of high-frequency stimulation (Fig. 6*A*). The prediction was that *Fmr1* KO neurons would not be able to sustain performance to the same extent as WT, because of a lack of new SVs being provided via ADBE (Nicholson-Fish et al., 2015). Cultures were stimulated with four trains of high-frequency APs (40 Hz 10 s) separated by 5-min intervals. WT neurons displayed a sequential decrease in the extent of the evoked sypHy response, consistent with a depletion of SVs available for exocytosis. When the same protocol was performed for *Fmr1* KO neurons, the sypHy response during the final stimulation was significantly lower when compared with WT (Fig. 6*B*). This suggests FMRP helps to sustain neurotransmitter release during increased neuronal activity via its control of ADBE.

BK channel activation corrects ADBE defects in *Fmr1* KO neurons

To determine the mechanism underlying the control of ADBE by FMRP, we examined the ability of specific loss of function

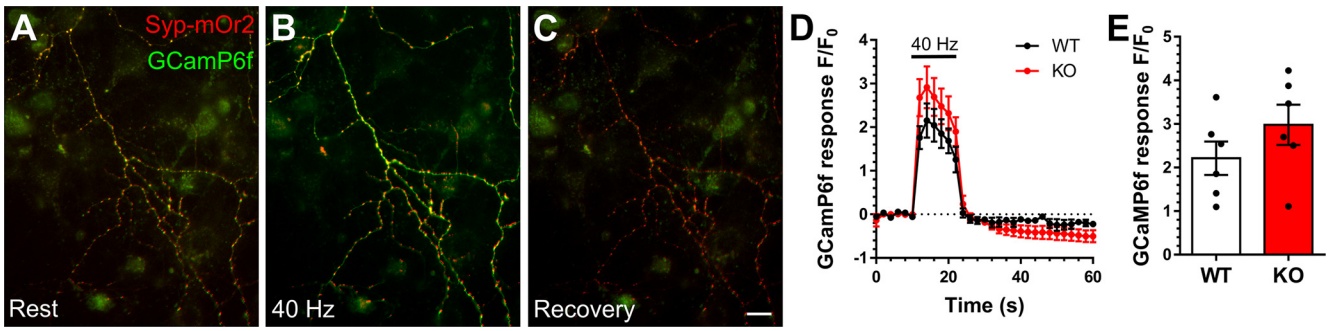

Figure 5. *Fmr1* KO hippocampal neurons do not display altered intracellular free calcium responses during high-frequency stimulation. Hippocampal neurons derived from either *Fmr1* KO or WT littermate controls were co-transfected with GCamP6f and synaptophysin-mOrange2 (Syp-mOr2) on DIV7 and imaged DIV15. Transfected neurons were challenged with a train of 400 APs (40 Hz). ***A–C***, Representative image of transfected neurons before (***A***, Rest), during (***B***, 40 Hz) and after (***C***, Recovery) stimulation. Scale bar: 1 µm. ***D***, Mean trace displaying the average GCamP6f fluorescent response of WT (black) and KO (red) at Syp-mOr2 positive puncta in response to stimulation (F/F_0 ± SEM). Bar indicates the period of stimulation. ***E***, Mean peak GCamP6f fluorescence response ± SEM during stimulation, $n = 6$ for both WT and KO, unpaired Student's *t* test, $p = 0.223$.

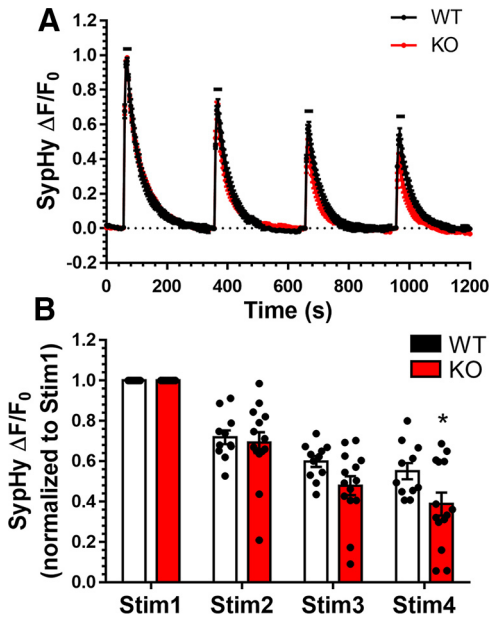

Figure 6. The ADBE defect in *Fmr1* KO neurons results in decreased presynaptic performance. Hippocampal neurons derived from either *Fmr1* KO or WT littermate controls were transfected with sypHy on DIV7 and imaged DIV13–DIV15. Transfected neurons were stimulated four times with 40 Hz 10 s at 5-min intervals, before exposure to an alkaline buffer (NH_4Cl). ***A***, Mean traces displaying the average sypHy fluorescent response traces of WT (black) and KO (red) hippocampal neurons is displayed ± SEM. Traces are $\Delta F/F_0$ and normalized to the sypHy peak response to the first train of APs. Bars indicate the periods of stimulation. ***B***, Mean sypHy peak heights for each 40-Hz 10-s stimulation, normalized to the first ± SEM WT $n = 11$ and KO $n = 14$, two-way ANOVA $^*p = 0.028$, Bonferroni's multiple comparison test, Stim1 $p > 0.99$, Stim2 $p > 0.99$, Stim3 $p = 0.15$, Stim4 $^*p = 0.02$.

mutants to rescue TMR-dextran uptake in *Fmr1* KO cultures. First, cultures from *Fmr1* KO rats or WT littermate controls were transfected with either an empty fluorescent mCer vector or mCer plus EGFP-FMRP (FMRP) 3 d before imaging. Overexpression of $FMRP_{WT}$ did not affect evoked TMR-dextran uptake in WT neurons (Fig. 7*A*,*B*), indicating that excess FMRP has no detrimental effect on ADBE. It also signifies that additional FMRP does not enhance ADBE, as observed with constitutively active Rab11 mutants (Kokotos et al., 2018). Importantly, $FMRP_{WT}$ expression was sufficient to fully rescue the impairment in TMR-dextran uptake in *Fmr1* KO neurons (Fig. 7*B*).

We exploited the ability of WT FMRP to fully rescue TMR-dextran uptake to perform molecular replacement studies using two loss of function mutants. These were: $FMRP_{I304N}$, which does not bind ribosomes (De Boulle et al., 1993), and $FMRP_{R138Q}$, which does not bind BK channels (Myrick et al., 2015; Kshatri et al., 2020; Fig. 7*C*). When these experiments were performed, $FMRP_{WT}$ restored TMR-dextran uptake in *Fmr1* KO cultures as previously observed (Fig. 7*D*). TMR-dextran uptake in $FMRP_{I304N}$ expressing neurons was not significantly different to neurons expressing $FMRP_{WT}$ (Fig. 7*D*). This indicates that FMRP-dependent control of protein translation is dispensable for ADBE. Interestingly, expression of $FMRP_{R138Q}$ failed to restore TMR-dextran uptake in *Fmr1* KO neurons, with levels equivalent to those observed with an empty vector (Fig. 7*D*). These results strongly suggest that FMRP controls ADBE through interactions with BK channels.

The absence of ADBE rescue by $FMRP_{R138Q}$ suggests that BK channel modulation by FMRP may be important for this endocytosis mode. Therefore, we investigated whether altering BK channel activity impacted ADBE. First, we determined whether enhancing channel activity with the activator NS 11021 could restore ADBE in *Fmr1* KO neurons. BK channel activation with NS 11021 did not affect TMR-dextran uptake in WT neurons when compared with a vehicle control (Fig. 8*A*). It did however restore TMR-dextran uptake in *Fmr1* KO neurons to WT levels (Fig. 8*A*). Therefore, activation of BK channels is sufficient to correct dysfunctional ADBE in *Fmr1* KO neurons.

To determine whether loss of BK channel function was responsible for defective ADBE in *Fmr1* KO neurons, we attempted to mimic the deficit using the BK channel antagonist Paxilline in WT hippocampal cultures. Interestingly, this maneuver did not impact activity-dependent TMR-dextran uptake (Fig. 8*B*). Taken together, these results suggest that while BK channel dysfunction is not responsible for ADBE defects in *Fmr1* KO neurons, BK channel activation can correct this fault.

Discussion

Loss of FMRP results in dysregulated translation of a specific cohort of mRNAs culminating in altered postsynaptic function (Darnell and Klann, 2013). However, FMRP also has noncanonical roles at the presynapse, particularly in the control of ion channel trafficking and activity. Disruption of these roles results in presynaptic dysfunction during intense neuronal activity (Deng et al., 2013; Wang et al., 2014; Ferron, 2016). We reveal that the absence of FMRP translates into a specific defect in ADBE, an endocytosis mode that is dominant during heightened neuronal activity. This defect results in reduced presynaptic performance during repetitive neuronal activity in *Fmr1* KO

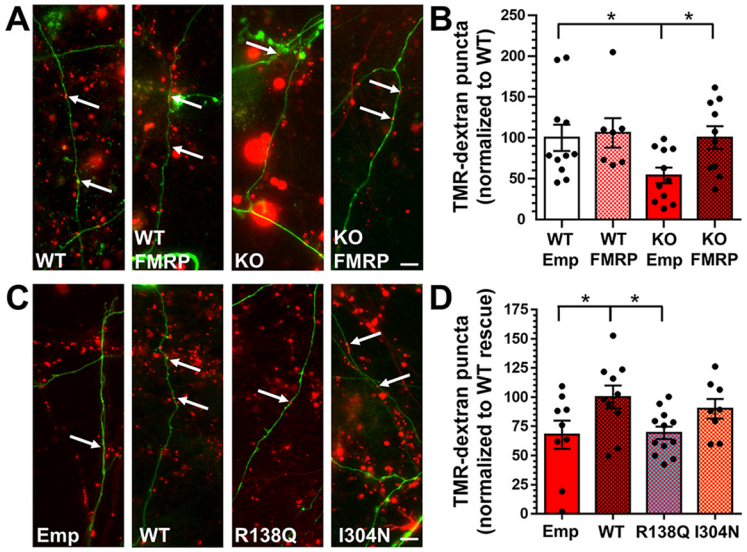

Figure 7. The R138Q FMRP mutant does not correct the ADBE defect in Fmr1 KO neurons. ***A***, ***B***, Hippocampal neurons derived from either *Fmr1* KO or WT littermate controls were transfected with mCerulean (Emp) or mCerulean and GFP-FMRP (FMRP) 3 d before imaging. On DIV13–DIV15, neurons were challenged with a 40-Hz 10-s AP train in the presence of 50 μM TMR-dextran. ***A***, Representative images of TMR-dextran uptake on axons transfected with empty or FMRP vectors, arrows indicate TMR-dextran puncta. Scale bar: 10 µm. ***B***, Mean TMR-dextran uptake per 100 µm of transfected axon is presented normalized to WT control ± SEM WT $n = 11$; WT FMRP $n = 7$; KO $n = 11$; KO FMRP $n = 10$, one-way ANOVA with Bonferroni multiple comparison test comparing WT empty and KO empty $^*p = 0.043$; and KO empty and KO FMRP $^*p = 0.048$. ***C***, ***D***, Hippocampal neurons derived from *Fmr1* KO embryos were transfected with mCerulean (Emp) or mCerulean and GFP-FMRP (WT), GFP-$FMRP_{R138Q}$ (R138Q), GFP-$FMRP_{I304N}$ (I304N) 3 d before imaging. On DIV13–DIV15, neurons were challenged with a 40-Hz 10-s AP train in the presence of 50 μM TMR-dextran. ***C***, Representative images of TMR-dextran uptake on axons transfected with empty or FMRP vectors, arrows indicate TMR-dextran puncta. Scale bar: 10 µm. ***D***, Mean TMR-dextran uptake per 100 µm of transfected axon is presented normalized to $FMRP_{WT}$ control ± SEM. Emp $n = 8$; WT $n = 10$; R138Q n =12; I304N $n = 8$, one-way ANOVA with Dunnett's multirole comparison test comparing all values to WT, empty $^*p = 0.043$, R138Q $^*p = 0.038$, I304N $p = 0.79$.

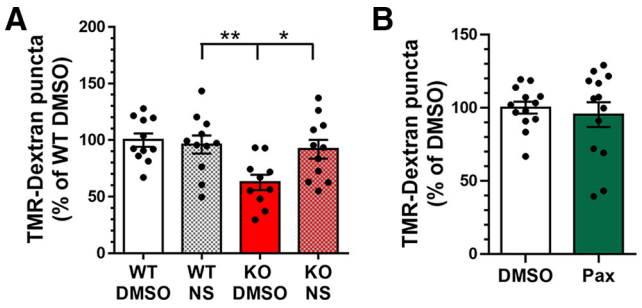

Figure 8. BK channel activation corrects ADBE defects in *Fmr1* KO neurons. ***A***, Hippocampal neurons from either *Fmr1* KO or WT littermate controls were incubated with DMSO or 10 μM NS 11021 (NS), and 50 μM TMR-dextran for 2 min before a 40-Hz 10-s stimulus on DIV13–DIV15. Mean TMR-dextran uptake as a proportion of total WT uptake ± SEM is displayed. WT DMSO $n = 11$; WT NS $n = 11$; KO DMSO $n = 10$; KO NS $n = 11$, one-way ANOVA with Bonferroni's multiple comparison test comparing WT DMSO and KO DMSO $^{**}p = 0.0039$; KO DMSO and KO NS $^*p = 0.032$; WT DMSO and KO NS $p > 0.9999$; WT DMSO and WT NS $p > 0.9999$. ***B***, WT hippocampal neurons were incubated with DMSO or 10 μM Paxilline (Pax) and 50 μM TMR-dextran for 2 min before a 40-Hz 10-s stimulus on DIV13–DIV15. Mean TMR-dextran uptake as a proportion of total WT uptake ± SEM is displayed. $n = 13$ for both DMSO and Pax, unpaired Student's t test $p = 0.62$.

neurons. Loss of BK channel interactions, but not channel activity, may be responsible for reduced ADBE, since $FMRP_{R138Q}$ failed to rescue function in KO neurons and BK channel inhibitors did not recapitulate the defect in WT neurons. Finally, the ability of BK channel activation to restore ADBE indicated that the defect may be an adaptation to hyperactivity in *Fmr1* KO neurons.

Previous studies have produced contradictory observations on SV numbers within CA1 nerve terminals in *Fmr1* KO mice *in situ* (Deng et al., 2011; Klemmer et al., 2011). Here, we provide a functional confirmation that the SV recycling pool is increased in *Fmr1* KO neurons. From first principles, ADBE inhibition should limit recycling SV pool size, however a complex relationship exists between ADBE and SV pools. For example, ADBE inhibition upregulates single SV pathways (Clayton et al., 2009, 2010; Smillie et al., 2013). Furthermore, VAMP4 is required for ADBE, but its selective trafficking independently impacts release probability, providing additional functional regulation than just SV reformation (Ivanova et al., 2021). Therefore, the increase in SV recycling pool size may be an adaptation to reduced ADBE, which occurs in ~40% of nerve terminals [vGLUT/vGAT labeling reveals 10% perform ADBE, whereas 25% of nerve terminals respond to a 40-Hz AP train: WT 28.9 ± 3.6; KO 24.6 ± 2.6 responsive synapses ($n = 13$ for both); Nicholson-Fish et al., 2016].

The increased recycling pool in *Fmr1* KO neurons did not result in increased number of SVs fusing during an AP train during either low or high-frequency stimulation, confirming the lack of a fundamental role for FMRP in SV exocytosis. This agrees with previous studies, where neurotransmitter release in intact hippocampal circuits from *Fmr1* KO mice was not different to WT after stimulation frequencies below 20 Hz (Deng et al., 2011). In contrast, studies in dorsal root ganglion neurons suggested that shRNA-induced depletion of FMRP enhanced SV fusion during high-frequency stimulation at 30°C (Ferron et al., 2014). Therefore, to confirm a lack of role for FMRP, we performed experiments at either physiological temperatures or by depleting FMRP with shRNA in hippocampal cultures. In both instances the absence of FMRP had no effect on SV exocytosis (K. Bonnycastle, unpublished observation). It is unclear why this disparity exists, however in primary cultures of rat hippocampal *Fmr1* KO neurons we observe no obvious SV fusion phenotype.

We observed specific and selective effects on ADBE in *Fmr1* KO neurons, which is the dominant form of endocytosis during high activity in both *in vitro* and *in vivo* (Clayton et al., 2008; Körber et al., 2012). TMR-dextran specifically reports ADBE because of size exclusion from single SVs (Clayton et al., 2008). Furthermore, ~90% of TMR-dextran puncta co-localize with the vital dye FM1-43 after high-frequency AP trains, indicating that this fluid phase marker it is only accumulated by active central nerve terminals (Clayton and Cousin, 2009). This uptake accurately reflects ADBE, since interventions that selectively block this endocytosis mode abolish TMR-dextran uptake (Clayton et al., 2009, 2010; Smillie et al., 2013; Morton et al., 2015). These same interventions also arrest the activity-dependent formation of HRP-labeled endosomes (Clayton et al., 2009, 2010; Morton et al., 2015). HRP-labeled endosomes reflect newly formed bulk endosomes, since the number of unlabeled presynaptic endosomes does

not change after stimulation, whereas additional HRP endosomes appear (Clayton et al., 2009, 2010; Smillie et al., 2013).

In this study, we observed that FMRP containing the I304N mutation fully restored TMR-dextran uptake in *Fmr1* KO neurons, while the R138Q mutation (which fully supports protein translation; Myrick et al., 2015; Kshatri et al., 2020) did not. Therefore, the inability of R138Q FMRP to rescue defective ADBE in KO neurons supports the hypothesis that presynaptic defects are translation-independent (Deng and Klyachko, 2016). The failure of R138Q FMRP to restore ADBE in *Fmr1* KO neurons could be because of the loss of BK channel regulation. BK channels control AP duration and shape, and in the absence of FMRP, *Fmr1* KO synapses display enhanced calcium influx because of AP broadening (Deng et al., 2013). However, this does not appear to be the case, since inhibition of BK channels in WT neurons does not recapitulate the defect in ADBE. An intriguing alternative is that the FMRP-dependent control of ADBE is independent of the modulation of BK channel activity. In this scenario, BK channels act as a docking station to place FMRP in the correct location to facilitate ADBE. Without this interaction, FMRP is mislocalized and unable to perform its role. In support, FMRP and its interaction partners, CYFIP2 and NUFIP2 are enriched on bulk endosomes formed via ADBE (Kokotos et al., 2018).

Another alternative is that the R138Q mutation results in a loss of FMRP function that is independent of BK channels. The FMRP N terminus interacts with at least 76 different proteins in non-neuronal cells (Taha et al., 2021), including CYFIP1/2 and NUFIP1/2 (Bardoni et al., 1999, 2003; Schenck et al., 2001). While the cellular role of most of these proteins are still unclear, CYFIP1/2 are key components of the Wave Regulatory Complex required for actin remodeling (Chen et al., 2010; Cioni et al., 2018). Actin dynamics are essential for optimal ADBE (Soykan et al., 2017), suggesting an additional noncanonical action of FMRP, similar to the actin-organizing role in SV endocytosis recently reported for Kv3.3 channels (Wu et al., 2021) Interestingly, *Cyfip1*$^{+/-}$ neurons display an increased recycling SV pool in primary culture (Hsiao et al., 2016), similar to our observations with *Fmr1* KO neurons in this study. Therefore, loss of FMRP function in ADBE may be because of disruption of parallel interactions within its N terminus.

The R138Q mutation is found in individuals presenting with ID and in some cases FXS phenotypes, seizures and autism (Collins et al., 2010; Myrick et al., 2015; Diaz et al., 2018; Sitzmann et al., 2018), although a direct link between the R138Q mutation and FXS has been questioned, since a cohort of individuals that display no discernable form of ID also carry this mutation (https://gnomad.broadinstitute.org). There may be explanations for this, however. For example, the cohort that carry the R138Q mutation may display a mild form of ID that was not detected in clinical assessments. Alternatively, other genetic modifiers may compensate for this mutation in these individuals, reducing its impact. Following this logic, this would mean that the R138Q FMRP mutation would have highly variable penetrance, dependent on the genetic composition of each individual subject. In support of a causal role, a recently generated knock-in mouse expressing the R138Q mutation displays cellular phenotypes and socio-cognitive defects similar to those observed in *Fmr1* KO mice (Prieto et al., 2021).

The correction of ADBE by BK channel activation suggests that the most likely mechanism for the observed reduction in ADBE is a compensatory or homeostatic mechanism to counteract the increased excitability in FXS and *Fmr1* KO models (Zhang et al., 2014; Booker et al., 2019; Das Sharma et al., 2020). In support, BK channel openers decrease hyperexcitability in *Fmr1* KO models both *in vitro* and *in vivo* by increasing hyperpolarization, resulting in decreased calcium influx in nerve terminals (Hébert et al., 2014; Zhang et al., 2014). However, the correction of ADBE via BK channel opening is not mediated at the level of calcium influx, since we demonstrate no change in evoked intracellular free calcium responses in *Fmr1* KO neurons.

A homeostatic reduction in ADBE in response to increased hyperexcitability would not be a homogenous adaptation across the brain, since neurons that display high firing rates would be disproportionately impacted. Therefore, even if reduced ADBE is not a causal mechanism in FXS, it may still be a valuable therapeutic intervention point to correct hyperexcitability in specific circuits (Booker et al., 2019; Das Sharma et al., 2020). Future studies are now required to determine whether modulation of ADBE can sculpt circuit activity in FXS (and other autism models that display hyperexcitability such as SynGAP haploinsufficiency disorder; Gamache et al., 2020). However, regardless of whether ADBE dysfunction contributes to FXS, the role of FMRP in the control of this key event provides valuable new information into the mechanisms of SV recycling that regulate presynaptic function.

References

Alabi AA, Tsien RW (2012) Synaptic vesicle pools and dynamics. Cold Spring Harb Perspect Biol 4:a013680.

Asiminas A, Jackson AD, Louros SR, Till SM, Spano T, Dando O, Bear MF, Chattarji S, Hardingham GE, Osterweil EK, Wyllie DJA, Wood ER, Kind PC (2019) Sustained correction of associative learning deficits after brief, early treatment in a rat model of fragile X syndrome. Sci Transl Med 11: eaao498.

Atluri PP, Ryan TA (2006) The kinetics of synaptic vesicle reacidification at hippocampal nerve terminals. J Neurosci 26:2313–2320.

Bardoni B, Schenck A, Mandel JL (1999) A novel RNA-binding nuclear protein that interacts with the fragile X mental retardation (FMR1) protein. Hum Mol Genet 8:2557–2566.

Bardoni B, Willemsen R, Weiler IJ, Schenck A, Severijnen LA, Hindelang C, Lalli E, Mandel JL (2003) NUFIP1 (nuclear FMRP interacting protein 1) is a nucleocytoplasmic shuttling protein associated with active synaptoneurosomes. Exp Cell Res 289:95–107.

Booker SA, Domanski APF, Dando OR, Jackson AD, Isaac JTR, Hardingham GE, Wyllie DJA, Kind PC (2019) Altered dendritic spine function and integration in a mouse model of fragile X syndrome. Nat Commun 10:4813.

Brown MR, Kronengold J, Gazula VR, Chen Y, Strumbos JG, Sigworth FJ, Navaratnam D, Kaczmarek LK (2010) Fragile X mental retardation protein controls gating of the sodium-activated potassium channel slack. Nat Neurosci 13:819–821.

Chanaday NL, Cousin MA, Milosevic I, Watanabe S, Morgan JR (2019) The synaptic vesicle cycle revisited: new insights into the modes and mechanisms. J Neurosci 39:8209–8216.

Chen TW, Wardill TJ, Sun Y, Pulver SR, Renninger SL, Baohan A, Schreiter ER, Kerr RA, Orger MB, Jayaraman V, Looger LL, Svoboda K, Kim DS (2013) Ultrasensitive fluorescent proteins for imaging neuronal activity. Nature 499:295–300.

Chen Z, Borek D, Padrick SB, Gomez TS, Metlagel Z, Ismail AM, Umetani J, Billadeau DD, Otwinowski Z, Rosen MK (2010) Structure and control of the actin regulatory WAVE complex. Nature 468:533–538.

Cheung G, Jupp OJ, Cousin MA (2010) Activity-dependent bulk endocytosis and clathrin-dependent endocytosis replenish specific synaptic vesicle pools in central nerve terminals. J Neurosci 30:8151–8161.

Cioni JM, Wong HH, Bressan D, Kodama L, Harris WA, Holt CE (2018) Axon-axon interactions regulate topographic optic tract sorting via CYFIP2-dependent WAVE complex function. Neuron 97:1078–1093.

Clayton EL, Cousin MA (2009) The molecular physiology of activity-dependent bulk endocytosis of synaptic vesicles. J Neurochem 111:901–914.

Clayton EL, Evans GJ, Cousin MA (2008) Bulk synaptic vesicle endocytosis is rapidly triggered during strong stimulation. J Neurosci 28:6627–6632.

Clayton EL, Anggono V, Smillie KJ, Chau N, Robinson PJ, Cousin MA (2009) The phospho-dependent dynamin-syndapin interaction triggers activity-dependent bulk endocytosis of synaptic vesicles. J Neurosci 29:7706–7717.

Clayton EL, Sue N, Smillie KJ, O'Leary T, Bache N, Cheung G, Cole AR, Wyllie DJ, Sutherland C, Robinson PJ, Cousin MA (2010) Dynamin I phosphorylation by GSK3 controls activity-dependent bulk endocytosis of synaptic vesicles. Nat Neurosci 13:845–851.

Collins SC, Bray SM, Suhl JA, Cutler DJ, Coffee B, Zwick ME, Warren ST (2010) Identification of novel FMR1 variants by massively parallel sequencing in developmentally delayed males. Am J Med Genet A 152A:2512–2520.

Cousin MA, Robinson PJ (2000) Ca(2+) influx inhibits dynamin and arrests synaptic vesicle endocytosis at the active zone. J Neurosci 20:949–957.

Darnell JC, Klann E (2013) The translation of translational control by FMRP: therapeutic targets for FXS. Nat Neurosci 16:1530–1536.

Das Sharma S, Pal R, Reddy BK, Selvaraj BT, Raj N, Samaga KK, Srinivasan DJ, Ornelas L, Sareen D, Livesey MR, Bassell GJ, Svendsen CN, Kind PC, Chandran S, Chattarji S, Wyllie DJA (2020) Cortical neurons derived from human pluripotent stem cells lacking FMRP display altered spontaneous firing patterns. Mol Autism 11:52.

De Boulle K, Verkerk AJ, Reyniers E, Vits L, Hendrickx J, Van Roy B, Van den Bos F, de Graaff E, Oostra BA, Willems PJ (1993) A point mutation in the FMR-1 gene associated with fragile X mental retardation. Nat Genet 3:31–35.

Deng PY, Klyachko VA (2016) Genetic upregulation of BK channel activity normalizes multiple synaptic and circuit defects in a mouse model of fragile X syndrome. J Physiol 594:83–97.

Deng PY, Sojka D, Klyachko VA (2011) Abnormal presynaptic short-term plasticity and information processing in a mouse model of fragile X syndrome. J Neurosci 31:10971–10982.

Deng PY, Rotman Z, Blundon JA, Cho Y, Cui J, Cavalli V, Zakharenko SS, Klyachko VA (2013) FMRP regulates neurotransmitter release and synaptic information transmission by modulating action potential duration via BK channels. Neuron 77:696–711.

Diaz J, Scheiner C, Leon E (2018) Presentation of a recurrent FMR1 missense mutation (R138Q) in an affected female. Transl Sci Rare Dis 3:139–144.

Feng Y, Absher D, Eberhart DE, Brown V, Malter HE, Warren ST (1997) FMRP associates with polyribosomes as an mRNP, and the I304N mutation of severe fragile X syndrome abolishes this association. Mol Cell 1:109–118.

Ferron L (2016) Fragile X mental retardation protein controls ion channel expression and activity. J Physiol 594:5861–5867.

Ferron L, Nieto-Rostro M, Cassidy JS, Dolphin AC (2014) Fragile X mental retardation protein controls synaptic vesicle exocytosis by modulating N-type calcium channel density. Nat Commun 5:3628.

Ferron L, Novazzi CG, Pilch KS, Moreno C, Ramgoolam K, Dolphin AC (2020) FMRP regulates presynaptic localization of neuronal voltage gated calcium channels. Neurobiol Dis 138:1094779.

Gamache TR, Araki Y, Huganir RL (2020) Twenty years of SynGAP research: from synapses to cognition. J Neurosci 40:1596–1605.

Granseth B, Odermatt B, Royle SJ, Lagnado L (2006) Clathrin-mediated endocytosis is the dominant mechanism of vesicle retrieval at hippocampal synapses. Neuron 51:773–786.

Hébert B, Pietropaolo S, Même S, Laudier B, Laugeray A, Doisne N, Quartier A, Lefeuvre S, Got L, Cahard D, Laumonnier F, Crusio WE, Pichon J, Menuet A, Perche O, Briault S (2014) Rescue of fragile X syndrome phenotypes in Fmr1 KO mice by a BKCa channel opener molecule. Orphanet J Rare Dis 9:124.

Hsiao K, Harony-Nicolas H, Buxbaum JD, Bozdagi-Gunal O, Benson DL (2016) Cyfip1 regulates presynaptic activity during development. J Neurosci 36:1564–1576.

Imig C, López-Murcia FJ, Maus L, García-Plaza IH, Mortensen LS, Schwark M, Schwarze V, Angibaud J, Nägerl UV, Taschenberger H, Brose N, Cooper BH (2020) Ultrastructural imaging of activity-dependent synaptic membrane-trafficking events in cultured brain slices. Neuron 108:843–860.

Ivanova D, Dobson KL, Gajbhiye A, Davenport EC, Hacker D, Ultanir SK, Trost M, Cousin MA (2021) Control of synaptic vesicle release probability via VAMP4 targeting to endolysosomes. Sci Adv 7:eabf3873.

Khayachi A, Gwizdek C, Poupon G, Alcor D, Chafai M, Cassé F, Maurin T, Prieto M, Folci A, De Graeve F, Castagnola S, Gautier R, Schorova L, Loriol C, Pronot M, Besse F, Brau F, Deval E, Bardoni B, Martin S (2018) Sumoylation regulates FMRP-mediated dendritic spine elimination and maturation. Nat Commun 9:757.

Klemmer P, Meredith RM, Holmgren CD, Klychnikov OI, Stahl-Zeng J, Loos M, van der Schors RC, Wortel J, de Wit H, Spijker S, Rotaru DC, Mansvelder HD, Smit AB, Li KW (2011) Proteomics, ultrastructure, and physiology of hippocampal synapses in a fragile X syndrome mouse model reveal presynaptic phenotype. J Biol Chem 286:25495–25504.

Kokotos AC, Peltier J, Davenport EC, Trost M, Cousin MA (2018) Activity-dependent bulk endocytosis proteome reveals a key presynaptic role for the monomeric GTPase Rab11. Proc Natl Acad Sci USA 115:E10177–E10186.

Körber C, Horstmann H, Sätzler K, Kuner T (2012) Endocytic structures and synaptic vesicle recycling at a central synapse in awake rats. Traffic 13:1601–1611.

Kshatri A, Cerrada A, Gimeno R, Bartolome-Martin D, Rojas P, Giraldez T (2020) Differential regulation of BK channels by fragile X mental retardation protein. J Gen Physiol 152:e201912502.

Leitz J, Kavalali ET (2016) Ca2+ dependence of synaptic vesicle endocytosis. Neuroscientist 22:464–476.

López-Murcia FJ, Royle SJ, Llobet A (2014) Presynaptic clathrin levels are a limiting factor for synaptic transmission. J Neurosci 34:8618–8629.

Mefford HC, Batshaw ML, Hoffman EP (2012) Genomics, intellectual disability, and autism. N Engl J Med 366:733–743.

Morton A, Marland JR, Cousin MA (2015) Synaptic vesicle exocytosis and increased cytosolic calcium are both necessary but not sufficient for activity-dependent bulk endocytosis. J Neurochem 134:405–415.

Myrick LK, Deng PY, Hashimoto H, Oh YM, Cho Y, Poidevin MJ, Suhl JA, Visootsak J, Cavalli V, Jin P, Cheng X, Warren ST, Klyachko VA (2015) Independent role for presynaptic FMRP revealed by an FMR1 missense mutation associated with intellectual disability and seizures. Proc Natl Acad Sci USA 112:949–956.

Nicholson-Fish JC, Kokotos AC, Gillingwater TH, Smillie KJ, Cousin MA (2015) VAMP4 is an essential cargo molecule for activity-dependent bulk endocytosis. Neuron 88:973–984.

Nicholson-Fish JC, Smillie KJ, Cousin MA (2016) Monitoring activity-dependent bulk endocytosis with the genetically-encoded reporter VAMP4-pHluorin. J Neurosci Methods 266:1–10.

Otsu N (1979) A threshold selection method from gray-level histograms. IEEE Trans Syst Man Cybern 9:62–66.

Prieto M, Folci A, Poupon G, Schiavi S, Buzzelli V, Pronot M, François U, Pousinha P, Lattuada N, Abelanet S, Castagnola S, Chafai M, Khayachi A, Gwizdek C, Brau F, Deval E, Francolini M, Bardoni B, Humeau Y, Trezza V, et al. (2021) Missense mutation of Fmr1 results in impaired AMPAR-mediated plasticity and socio-cognitive deficits in mice. Nat Commun 12:1557.

Richards DA, Guatimosim C, Betz WJ (2000) Two endocytic recycling routes selectively fill two vesicle pools in frog motor nerve terminals. Neuron 27:551–559.

Sankaranarayanan S, Ryan TA (2001) Calcium accelerates endocytosis of vSNAREs at hippocampal synapses. Nat Neurosci 4:129–136.

Schenck A, Bardoni B, Moro A, Bagni C, Mandel JL (2001) A highly conserved protein family interacting with the fragile X mental retardation protein (FMRP) and displaying selective interactions with FMRP-related proteins FXR1P and FXR2P. Proc Natl Acad Sci USA 98:8844–8849.

Sitzmann AF, Hagelstrom RT, Tassone F, Hagerman RJ, Butler MG (2018) Rare FMR1 gene mutations causing fragile X syndrome: a review. Am J Med Genet A 176:11–18.

Smillie KJ, Pawson J, Perkins EM, Jackson M, Cousin MA (2013) Control of synaptic vesicle endocytosis by an extracellular signalling molecule. Nat Commun 4:2394.

Soykan T, Kaempf N, Sakaba T, Vollweiter D, Goerdeler F, Puchkov D, Kononenko NL, Haucke V (2017) Synaptic vesicle endocytosis occurs on multiple timescales and is mediated by formin-dependent actin assembly. Neuron 93:854–866.

Taha MS, Haghighi F, Stefanski A, Nakhaei-Rad S, Kazemein Jasemi NS, Al Kabbani MA, Görg B, Fujii M, Lang PA, Häussinger D, Piekorz RP,

Stühler K, Ahmadian MR (2021) Novel FMRP interaction networks linked to cellular stress. FEBS J 288:837–860.

von Gersdorff H, Matthews G (1994) Inhibition of endocytosis by elevated internal calcium in a synaptic terminal. Nature 370:652–655.

Wang XS, Peng CZ, Cai WJ, Xia J, Jin D, Dai Y, Luo XG, Klyachko VA, Deng PY (2014) Activity-dependent regulation of release probability at excitatory hippocampal synapses: a crucial role of fragile X mental retardation protein in neurotransmission. Eur J Neurosci 39:1602–1612.

Watanabe S, Rost BR, Camacho-Pérez M, Davis MW, Söhl-Kielczynski B, Rosenmund C, Jorgensen EM (2013) Ultrafast endocytosis at mouse hippocampal synapses. Nature 504:242–247.

Wenzel EM, Morton A, Ebert K, Welzel O, Kornhuber J, Cousin MA, Groemer TW (2012) Key physiological parameters dictate triggering of activity-dependent bulk endocytosis in hippocampal synapses. PLoS One 7:e38188.

Wu XS, Wu LG (2014) The yin and yang of calcium effects on synaptic vesicle endocytosis. J Neurosci 34:2652–2659.

Wu XS, Subramanian S, Zhang Y, Shi B, Xia J, Li T, Guo X, El-Hassar L, Szigeti-Buck K, Henao-Mejia J, Flavell RA, Horvath TL, Jonas EA, Kaczmarek LK, Wu LG (2021) Presynaptic Kv3 channels are required for fast and slow endocytosis of synaptic vesicles. Neuron 109:938–946.

Zhang N, Gordon SL, Fritsch MJ, Esoof N, Campbell DG, Gourlay R, Velupillai S, Macartney T, Peggie M, van Aalten DM, Cousin MA, Alessi DR (2015) Phosphorylation of synaptic vesicle protein 2A at Thr84 by casein kinase 1 family kinases controls the specific retrieval of synaptotagmin-1. J Neurosci 35:2492–2507.

Zhang Y, Bonnan A, Bony G, Ferezou I, Pietropaolo S, Ginger M, Sans N, Rossier J, Oostra B, LeMasson G, Frick A (2014) Dendritic channelopathies contribute to neocortical and sensory hyperexcitability in Fmr1(-/y) mice. Nat Neurosci 17:1701–1709.